3D Coronal Structures and Magnetic Field during a Total Solar Eclipse 29 March 2006.

P. Ambrož[1] · **M. Druckmüller**[2] ·
A.A. Galal[3] · **R.H. Hamid**[3]

Abstract The good quality of the observing sequence of about 60 photographs of the white-light corona taken during the total solar eclipse observations on 29 March 2006, in Al Sallum, Egypt, enable us to use a new method of image processing for enhancement of the fine structure of coronal phenomena. We present selected magnetic field lines derived for different parameters of the extrapolation model. The coincidence of the observed coronal white light fine structures and the computed field-line positions provides a 3D causal relationship between coronal structures and the coronal magnetic field.

Keywords: Eclipse Observations; Corona, Structures; Magnetic fields, Corona

1. Introduction

Substantial changes in the image of the solar white-light corona observed during many total solar eclipses over the course of the last two centuries lead to a close relationship between the phase of the solar activity cycle and the global shape of the solar corona (Loucif and Koutchmy, 1989). Many eclipse photographs show a distinct variation of brightness of the corona as well as in the position angle around the solar limb. Significant changes of shape and the internal fine structure of the corona are related to cycles of solar activity and with the structure of the solar magnetic field. Here we describe the coronal phenomena, mainly in the middle and outer corona. The inner corona is, in a radial direction, characterized by a very steep gradient of brightness, with a dynamical range of up to 1:10 000 or

---

[1] Astronomical Institute Acad. Sci. Czech Republic, 25165
Ondřejov, The Czech Republic
email: pambroz@asu.cas.cz
[2] Institute of Mathematics, Faculty of Mechanical
Engineering, Brno University of Technology, 619 69 Brno,
The Czech Republic
email: druckmuller@fme.vutbr.cz
[3] National Research Institute of Astronomy and Geophysics
(NRIAG), Helwan, Egypt
email: agalal@nriag.sci.eg
email: rabab_helal@yahoo.com

more. Observing programs prepared for total eclipse expeditions during the last 40 years were, among other objectives, characterized by attempts to eliminate the steep gradient of brightness in the coronal image. Application of radial filters just in front of the photographic emulsion as well as a recently used approach to take many photos with a continuously increasing and decreasing exposure time are ways to eliminate the high brightness radial gradient and large-scale diffuse structures. A goal of our study is to compare the observed fine structures with calculated field lines when possible. We suppose that the open and closed structures in the corona are controlled by a large-scale magnetic field and by the expanding solar wind. The 29 March 2006 total solar eclipse was recently studied by Wang *et al.* (2007) and Pasachoff *et al.* (2007). Our approach to the coronal structure analysis is similar in some respects however primary solar observations and magnetic field calculations are different and are presented herefor the first time.

2. Observing Materials

2.1. Corona Observation and Processing

Observations of the white light corona were obtained by the expedition of the Solar Laboratory of the National Research Institute of Astronomy and Geophysics (NRIAG) of Egyptian Academy of Sciences in Helwan, Egypt, during the 29 March 2006 total solar eclipse (Galal *et al.*, 2007). The eclipse observations were carried out on the northwest coast of the Mediterranean Sea near Al Sallum on the Egyptian–Libyan border and about 4.5 km from the coastline. The site was located at N $31°34'03''$ and E $25°07'22''$ at an elevation 179 meters. At second contact at 10:40 UT, the Sun was at an altitude of $62°$. Totality lasted for 235 seconds under good clear sky conditions.

The observing instrument used for the white light photography of the eclipse corona consisted of an apochromatic refractor (William Optics) with 110/775 mm fluorite triplet lens, driven on a Losmandy G11 equatorial mount and was equipped with a Canon EOS 1Ds Mark II Digital SLR Camera with 16.7 mega-pixel full frame (36×24mm) CMOS sensor. The observing procedure was controlled by a computer and during the 200 seconds long observing period 60 photographs with different exposure times were taken. The numerical processing method, based on the application of adaptive filters, was recently developed by Druckmüller and described in detail by Druckmüller, Rušín, and Minarovjech (2006). The processed image allows us to study both small- and large-scale coronal structures which sometimes remain invisible on the original images because of the very high dynamic range of coronal brightness.

The necessary condition for application of the method is to use a set of photographs taken during the eclipse with a wide range of exposure times from 0.001 second to a few seconds, precisely aligned and combined in the final picture. The successful method of processing them prescribes some rules also for planning of the observing procedure. For purposes of the present study, however, we did not anticipate this kind of processing and we approached the image processing only
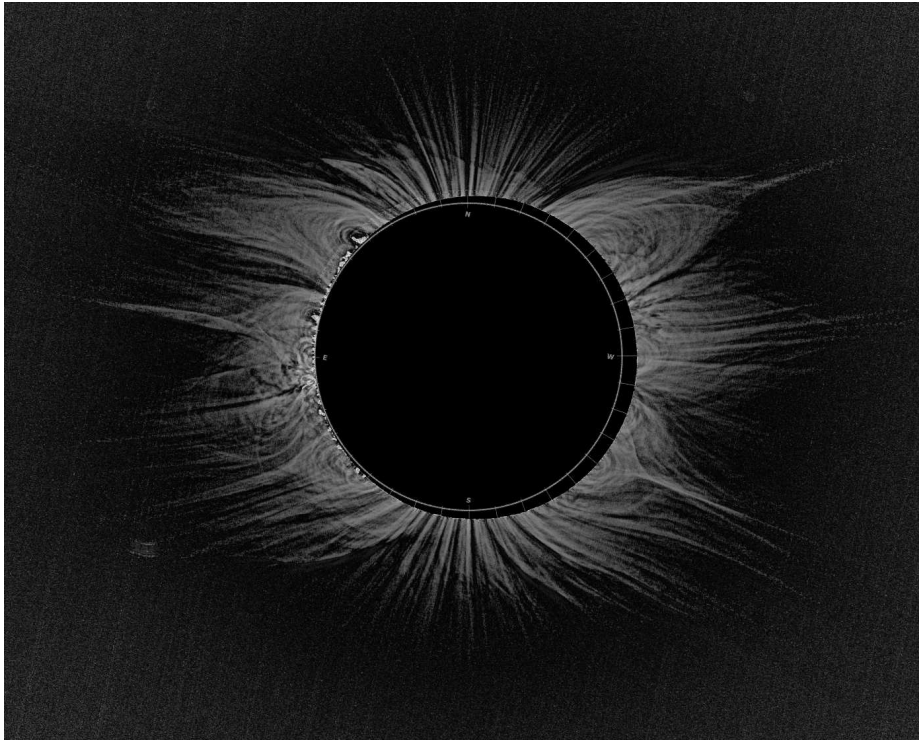
Figure 1. Processed image of the white light corona from 29 March 2006 observed at Al Sallum, Egypt.

after observing of the solar eclipse. Therefore, not all conditions necessary for processing methods were satisfied completely during the observations. The main disadvantages are as follows:

- Due to a mistake during the observing program preparation, the photos with long exposure times (for $ISO = 100$ and $f/7$ longer than 0.3 second) were omitted. The processed image of the outer corona contains therefore an significant noise component due to a low signal-to-noise ratio.
- The choice of the exposure times of images in chronological order does not continuously increase and a sudden change is present. Such a jump cannot be improved later because for each exposure time only a narrow annulus around the Moons image contributes to a finally processed image. This effect causes the relatively low quality of limb details on the east side of the solar limb.
- Problems on the west limb are mainly due to a few long exposed photos just before the third contact (C3). The photographs near the limb are overexposed, saturated and therefore the information content in this part of the corona is zero. The final image of the Moon was, therefore, located at C2 + five seconds. The accuracy of the coronal image position angle is better than $\pm 0.1°$.

- Only a few photographs are degraded by dust on the sensor or by other factors (distortion by seeing or unsharp images) and therefore out of a total of 60 images about 40 photographs were used for processing.

It is evident that the careful planning of the whole observation procedure during the totality period is crucial for final image processing and for the image quality of fine coronal structures.

We assume that the shape of the fine structures is determined by a coronal magnetic field. It is necessary for the study of any correspondence of the observed fine coronal structures with extrapolated coronal magnetic-field lines to understand fully the image processing techniques used for image creation. For example, the numerically created radial filter based on rotational image blurring enhances radial structures only and tangential structures remain invisible. Therefore using this type of radial filter may change the appearance of loop structures to open line ones and ignorance of this fact may lead to totally incorrect interpretation. The main aim of our numerical image processing was to attenuate the amplitude of low spatial frequencies in the Fourier spectrum and amplify the amplitude of high spatial frequencies without changing the phase spectrum and without artifacts caused by an extreme brightness discontinuity at the lunar edge. The resulting image from the photometric point of view does not correspond to reality; on the other hand it is very near to what human vision would see if it were able to manage the extreme brightness ratio and if the structure contrast was higher than in reality. Human vision as a differential analyzer has no ability to determine brightness; it is able only to compare the brightness of a picture element with its neighborhood.

The processed image of the corona provides information about a density difference. However, it is dramatically different from unprocessed pictures, which relate to the density distribution in the corona (Woo and Druckmüllerová , 2008).

2.2. Numerical Extrapolation of the Coronal Magnetic Field

Extrapolation of the magnetic field measured in the photosphere into the coronal space is generally possible by numerous ways depending on the accepted physical or numerical model. The potential model with or without a source surface (Altschuler and Newkirk, 1969; Schatten, 1971; Wang, Sheeley, 1992), quasi-potential models with a horizontal current (Zhao and Hoeksema, 1993), introducing the cusp surface (Zhao and Hoeksema, 1994) as well as linear force free (Nakagawa and Raadu, 1972) represent the category of models in which the dynamical expansion of the corona is not explicitly included. The outer boundary is characterized by the value of the magnetic potential. It is not very distant from the solar surface (from 2 to $4.5R_\odot$) and sometimes the value of the radius R_{ss} varies above the Sun (Schulz, Frazier, and Bouchner, 1978). The magnetic field in the photosphere is usually derived from daily measurements of the longitudinal component with specific assumptions about the radial surface field orientation. Another branch of the extrapolation model is based on a numerical solution of the set of MHD equations (Mikic *et al.*, 1999) or they are extrapolated from magnetic measurements of the full vector magnetic field in the solar photosphere (Wiegelmann, 2004).

Our aim is to model the 3D distribution of the magnetic field in the corona on the basis of solution of the magneto-static atmosphere with horizontal electric current. The model presented by Bogdan and Low (1986) is built on the magneto-static equilibrium in a solar atmosphere with the presence of a coronal current, however in a very specific form. In the model it is assumed that the solar atmosphere possesses electric current densities distributed continuously in space and that current is directed perpendicular to the gravitational force. This class of the model is called a model with a horizontal current. The influence of the solar wind, represented by expanding coronal plasma into interplanetary space, is the reason that at some distance from solar center the orientation of the solar magnetic field is only radial. The limiting distance is called source surface R_{ss}. The numerical model for computation of the large-scale magnetic field in 3D with horizontal current and with a source surface (HCSS) was used by Zhao and Hoeksema (1993)

$$\mathbf{B} = -\eta(r)\frac{\partial \Phi}{\partial r}\bar{r} - \frac{1}{r}\frac{\partial \Phi}{\partial \theta}\bar{\theta} - \frac{1}{\sin\theta}\frac{\partial \Phi}{\partial \phi}\bar{\phi}, \tag{1}$$

where the $\eta(r) = (1 + \frac{a}{r})^2$ and a is a free parameter related to the scale length of the horizontal electric current. The generating function $\Phi(r, \theta, \phi)$ is

$$\Phi = \sum_{n=1}^{N=19}\sum_{m=0}^{n} R_n(r)P_n^m(\cos\theta)F_n^m(\phi), \tag{2}$$

where $P_n^m(\cos\theta)$ are associated Legendre polynomials,

$$F_n^m(\phi) = g_n^m\cos m\phi + h_n^m\sin m\phi, \tag{3}$$

and the radial dependence is

$$R_n(r) \;=\; R_\odot^2 \big[\frac{1}{(r+a)^{n+1}} - \frac{(r+a)^n}{(R_{ss}+a)^{2n+1}}\big]/$$
$$\big[\frac{n+1}{(R_\odot+a)^n} + \frac{n(R_\odot+a)^{n+1}}{R_{ss}+a)^{2n+1}}\big]. \tag{4}$$

The spherical harmonic coefficients g_n^m and h_n^m, where n is a principal index, are used from observations of Wilcox Solar Observatory (WSO) of Stanford University and are available on http:\\wso.stanford.edu/forms/prgs.html as a result of the radial method. They are derived from the daily measured magnetic field for which it is assumed that the magnetic vector is radial in the photosphere. The spatial resolution of the photospheric magnetic field is limited by the maximal principal index n of the used spherical harmonic coefficients.

The role of the source surface in the HCSS model is to simulate a radial limit above which the coronal magnetic field remains only radial. This condition follows directly from its definition. From a mathematical point of view the
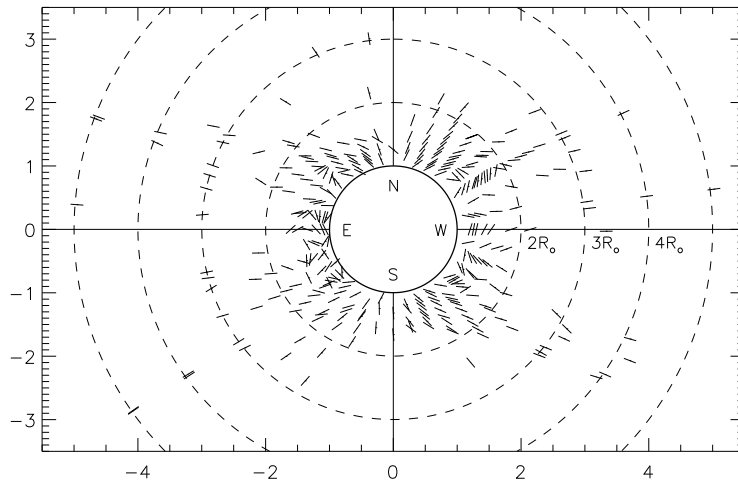
Figure 2. Demonstration of the orientation of selected fine structures as observed during the 29 March 2006 total solar eclipse.

source surface represents the outer boundary of the extrapolation space. With increasing height above the solar photosphere the contribution from high-order spherical harmonics decreases and the near source surface's only contribution is from the first three spherical harmonics. The radius of the source surface characterizes how rapidly the transverse field components presented in the low corona is attenuated.

R_{ss} is the heliocentric distance of the source surface and is a free parameter. We are able to determine a reasonable value of R_{ss} from the corona fine-structure observation. Orientation of the magnetic field as projected onto the sky plane can be deduced from the orientation of the fine fibrils and threads in observed corona. The processed picture of the eclipse corona in Figure 1 was used for determination of the magnetic vector orientation in the observing plane and results are shown in Figure 2. In an annulus between $1.0R_{\odot} < r < 3.0R_{\odot}$ the measuring points were determined on intersections of fine coronal structures with discrete radial lines separated by $10°$ in position angle. At each point the angle between the tangent to a coronal structure and the radial line is determined. Above this region the inclination was measured at points displaced on circles with radii 3, 4, and $5R_{\odot}$. This approach provides discrete steps in radius, however, all structures are measured.

We present in Figure 3 statistics of the dependence of the inclination of the coronal structures from the radial direction on the radial distance. The maximal scatter of the inclinations from a radial direction is below $2.0R_{\odot}$, however also in the distance range 2.5 - $3.0R_{\odot}$ the scatter in range $\pm20°$. At $4.0R_{\odot}$ the inclination is about $\pm10°$ or lower. We expect that above this height, as observed for more extended structures by SOHO/LASCO-C2, only the radial component of the coronal magnetic field is present.

For $R_{ss} = 2.5R_{\odot}$ the condition of only radial orientation is generally never satisfied. For the large-scale steady state we used the extrapolated magnetic
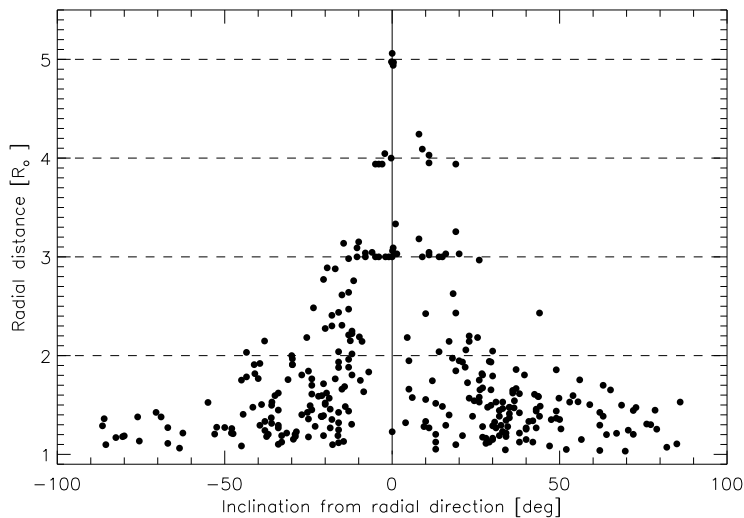
Figure 3. Distribution of the inclination angle of the coronal fine structures according to radial distance from the Sun's center. Negative inclination is measured clockwise from radial.

structure. Above the standard radius, $R_{ss} = 4.0 R_\odot$, we assume that we find only radial magnetic field.

Also the determination of the length scale a for the horizontal current density distribution of the observed structures was important for this choice. The magnetostatic approximation of the coronal model is justified by the persistence, or very small changes, of large-scale structures in the photosphere for longer than one solar rotation. The model requires the electric current density to be distributed continuously in space with a length scale of a and currents to be perpendicular to the gravitational force. The free parameter a must be kept within a limited range of values to obtain reasonable plasma properties. Setting $a = 0$ gives the potential field solution with no current in coronal space. Calculations with $a < 0$ correspond to radial compression of the atmosphere, whereas $a > 0$ is an expansion of the atmosphere from the potential state. The increased value a causes a proportional increase of the height of the summits of the computed field line arcades and loops, as documented in Figure 4. The value of a is assumed to be constant throughout the corona and this has a significant influence on the geometrical shape of the computed magnetic field lines when other input values are conserved.

3. Coronal Structures and Magnetic Field

Coronal structures observed in the last third of the last century by different methods were interpreted in relation to the image spatial resolution. A nearly diffuse image of coronal structures interpreted as the continuous but inhomogeneous upper layer of the solar atmosphere in the epoch before *Skylab* was changed after this mission and the coronal structure was considered mainly as the composition
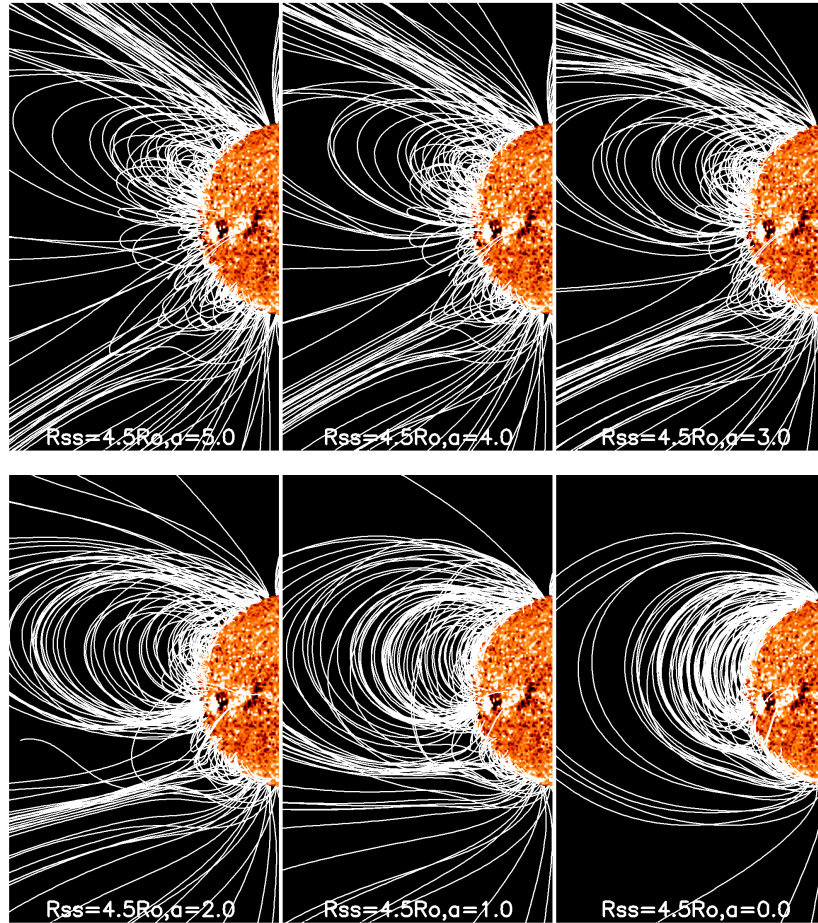
Figure 4. Extrapolated magnetic field according to the HCSS model for a given source surface radius $R_{ss} = 4.0R_{\odot}$. The value a is changed in the range from 0 to 5, whereas the photospheric magnetic field from WSO measurements for CR2041 remain constant.

of many loops and arcades as well as the nearly empty coronal holes. For white-light observations, the successful attempt made by November and Koutchmy (1996) shows that in white light the corona also contains extremely narrow fine structures. New observations of the white-light corona after 1991 and an application of digital sensors as well as new methods of digital processing opens the possibility of obtaining very fine images of many coronal structures.

The processed image of the eclipse corona in Figure 1 looks like a composition of fine details; however, it provides a complex organized system of fine structures, rays, threads, and ropes. The finest threads have a characteristic diameter from 5 Mm to more frequently 20 Mm. The finest structures observed above the active zone are extremely chaotic due to the overlapping of many individual loops, arches, and rays. We tried to make decomposition of the interesting but too complex image with the help of the model of an extrapolated magnetic field. The aim is to obtain 3-D distribution of the individual observed structures.
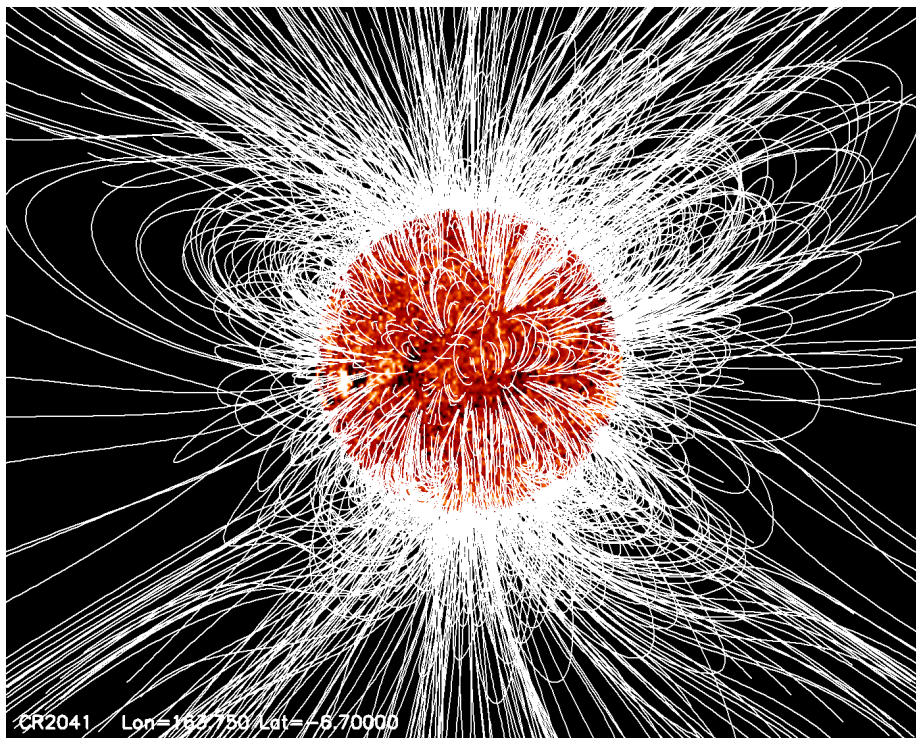
Figure 5. Extrapolated magnetic field for the position of the solar corona during the 29 March 2006 eclipse. Field lines are computed for $R_{ss} = 4.0R_{\odot}$, and $a = 3.0$ from regularly distributed grid points in the photosphere. Initial points for field lines integration in heliographic coordinates have the increment $5°$ in both longitude and latitude except poles.

The extrapolated magnetic-field lines with starting points distributed regularly according to a simple rule (orthogonal mesh) in the photosphere usually do not coincide with displayed coronal structures also in the case of general structure of the magnetic field is known. In the extrapolation procedure it is necessary to prescribe the starting point for 3D numerical integration of each the field line. A general physical method is not available for determining which computed field lines will be enveloped (or magnetic tubes filled) by sufficiently dense plasma and which will not. So we usually compute an extensive set of field lines as shown in Figure 5, however only a small part of them exhibit coronal threads, fibrils or ropes which can be observed in a short time interval of totality as bright coronal structures. For the analysis we selected from many computed field lines only those coinciding with existing observed fine structures of coronal plasma. It is necessary to have detailed information about the field structure in the corona. For this purpose the increment of field lines was $1°$ in both heliographic longitude and latitude. Comparison of observed coronal fine structures was made for each meridian cut in the neighborhood of the limb. Eclipse photos also reveal coronal structures for which we are not able to find corresponding extrapolated field lines. We will discuss this problem in Section 4.
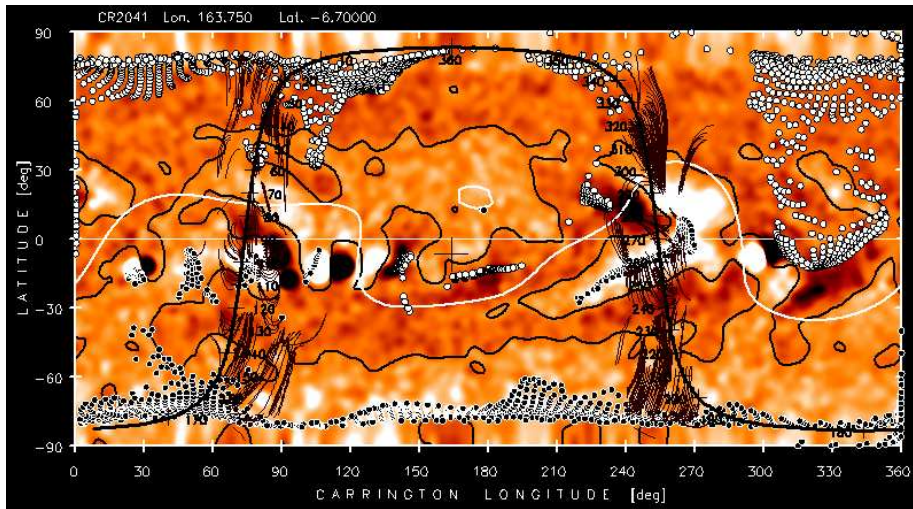
Figure 6. Magnetic synoptic map drawn with scaled limb. The selected field lines plotted in Figures 9 and 10 are projected onto the photosphere. The circles represent foot points of the open field lines white-positive and black-negative polarities in the photosphere. The white line shows the position of the neutral line (heliospheric current sheet) on the source surface for $R_{ss} = 4.0R_{\odot}$. The black bold limb-line is calibrated in position angle values, measured around the limb from the north pole counterclockwise.

3.1. Open Structures

Many fine open structures are present on the processed photo in Figure 1. The polar plumes around both poles are created by very subtle rays mainly in the upper half of their height (from about $0.3 - 0.5R_{\odot}$ above the solar limb). Below this limit, close to the limb, they appear as overlapped by the projection of another set of structures. We seriously suspect that this system is diverging from foot points rooted in polar regions in a range from $15°$ to $25°$ in latitude from both poles on both front and back sides of the limb line, close to the outer boundaries of the polar coronal holes. The upper limit of the overlapping structures is given by the apparent summit points of rays, projected into the observing plane. This limit coincides with line-of-sight projection of near pole boundaries of the large-scale structures observed in the mid-latitudes on both east and west limbs.Relationship of polar plumes with small-scale enhancements in EUV corona from the SOHO/EIT observations and their temporal stability was studied by Pasachoff *et al.* (2008). They are also extended on both the visible and far sides of the Sun. The visibility of this phenomenon is probably also enhanced by the processing method.

The open-ray-like structures outside the polar regions are nearly radially oriented above the distance $3.5 - 4.0R_{\odot}$ from the solar center. Below this limit the orientation of the open structures varies and their footpoints in the photosphere are concentrated into spatially limited regions. Usually the regions in the photosphere coincide with unipolar magnetic regions in the corona with coronal holes and with coronal plumes (Wang and Muglach, 2008). On the processed image,

the open white-light fine coronal structures overlap also many closed structures with an arch-like shape. The small optical thickness of the corona results in the fine coronal structures being transparent and the contributions from different systems along the observing lines are projected together into the observing plane. The projected combination of the open and closed fine structures, however, does not support the conclusion of Woo (2006) that very fine open structures extend radially from the entire Sun.

The composite synoptic chart in Figure 6 shows a topology of the large-scale magnetic field averaged from the SOHO/MDI data and the position of the limb line with calibrated bars of the position angle. In the map are also drawn the position of magnetic inversion lines in the photosphere, calculated footpoints of the open field lines, selected field lines identified above both solar limbs, and the calculated position of the heliospheric current sheet on the source surface, all according to our extrapolation model.

The open field lines are numerically integrated from points on the source surface down to the photosphere. The increment of both heliographic coordinates on the source surface is $5°$. Their footpoints for $R_{ss} = 4.0R_{\odot}$ are drawn on a magnetic synoptic chart in Figure 6 by a set of small circles. Black circles refer to negative polarity, the white circles to positive polarity. Only a very small area of the solar photosphere is related to interplanetary space. The position of the magnetic inversion line dividing both polarities on the source surface is depicted by the white line.

The model for $R_{ss} = 2.5R_{\odot}$ also gives for open structures also not a bad coincidence in the low corona. However, the shape and amount as well as an extension of the regions with field line footpoints covers a more extended area than observed coronal holes, presented in Figure 5c in Wang *et al.* (2007). This disagreement in the photosphere as well as the poor agreement for the corona above $2.5R_{\odot}$ make use of $R_{ss} = 4.0R_{\odot}$ favorable.

3.1.1. Open Structures on the East Limb

A projection of the open field lines on the east hemisphere is shown in Figure 7. As described in the figure caption, two values of the source surface (a) $R_{ss} = 2.5R_{\odot}$ and (c) $R_{ss} = 4.0R_{\odot}$ are demonstrated. In both cases the open rays forming funnel-shaped structures are concentrated into three separate systems which are divided by two coronal closed arch-shaped phenomena.

The field lines close the northern pole, labeled as "A" and similarly between labels "K" and "L" on the south are rooted in corresponding polar coronal holes.

The open field lines above the east limb in the north hemisphere presented in Figure 6 are rooted in two different regions of positive polarity (coronal holes), one in front (about $25°$ in longitude) and labeled as "BC". A second small hole is nearly on the limb line, labeled as "DE" .

An extrapolated heliographic current sheet (HCS) on the source surface in the observing plane is located at latitude N17° (position angle 75°), independent of both values R_{ss}. The field-line systems southward from HCS are related to the negative polarity. In the equatorial region there are also two footpoint regions rooted in photosphere along the line of sight in front (21°) and behind (-6°) the
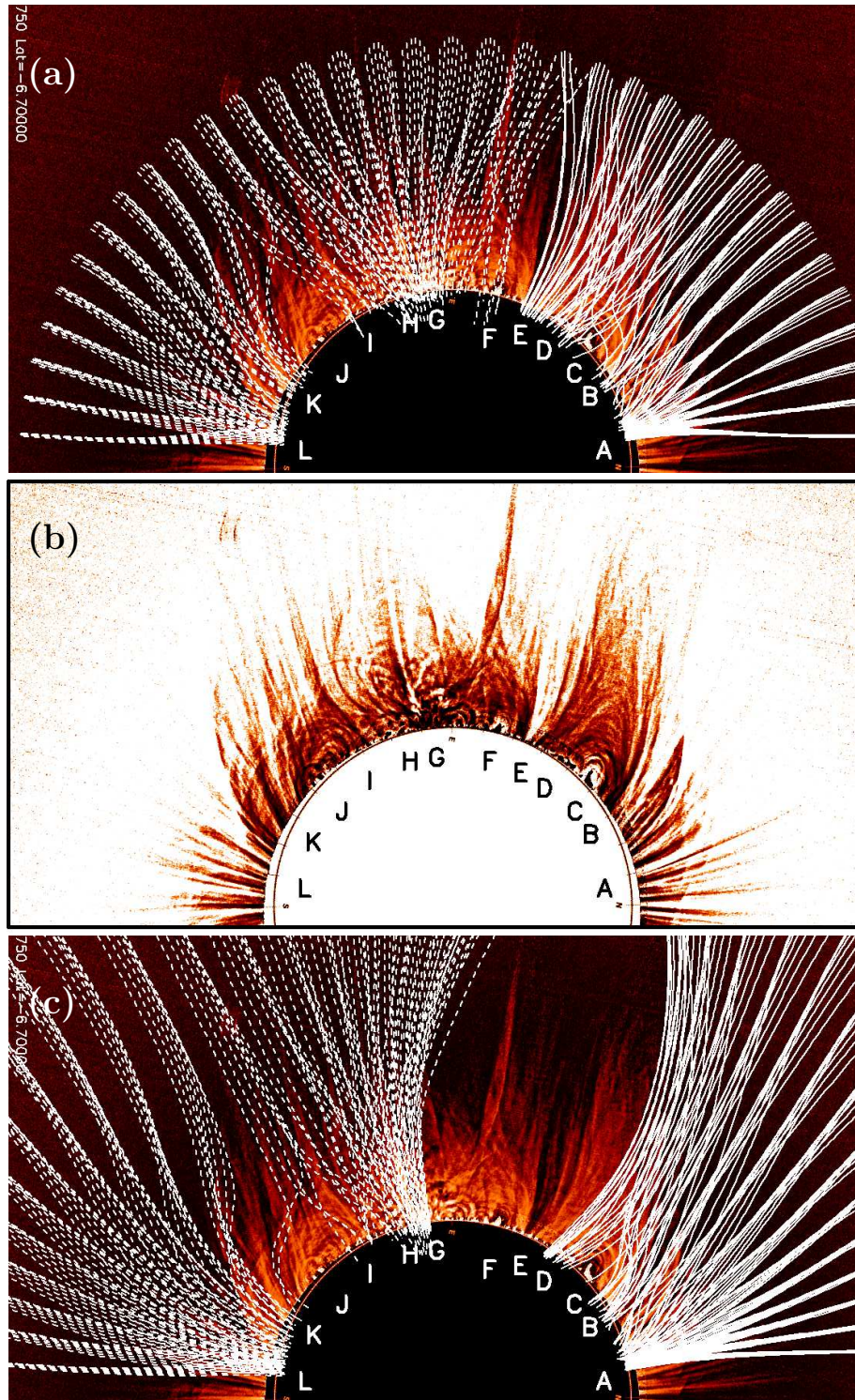
Figure 7. Open field lines are computed in a narrow $\pm 20°$ broad sector above the east limb in contrast with Figures 10 and 11 . Field lines based on the HCSS model for source surface radius (a) $R_{ss} = 2.5 R_\odot$ and (c)$R_{ss} = 4.0 R_\odot$ from grid points on the source surface with the increment $5°$ in latitude and longitude. Field lines related to negative polarity in the photosphere are indicated by dashed lines. Graph (b) shows processed coronal structures. The north pole is on the right and photos show position angles in range from $0°$ to $180°$.
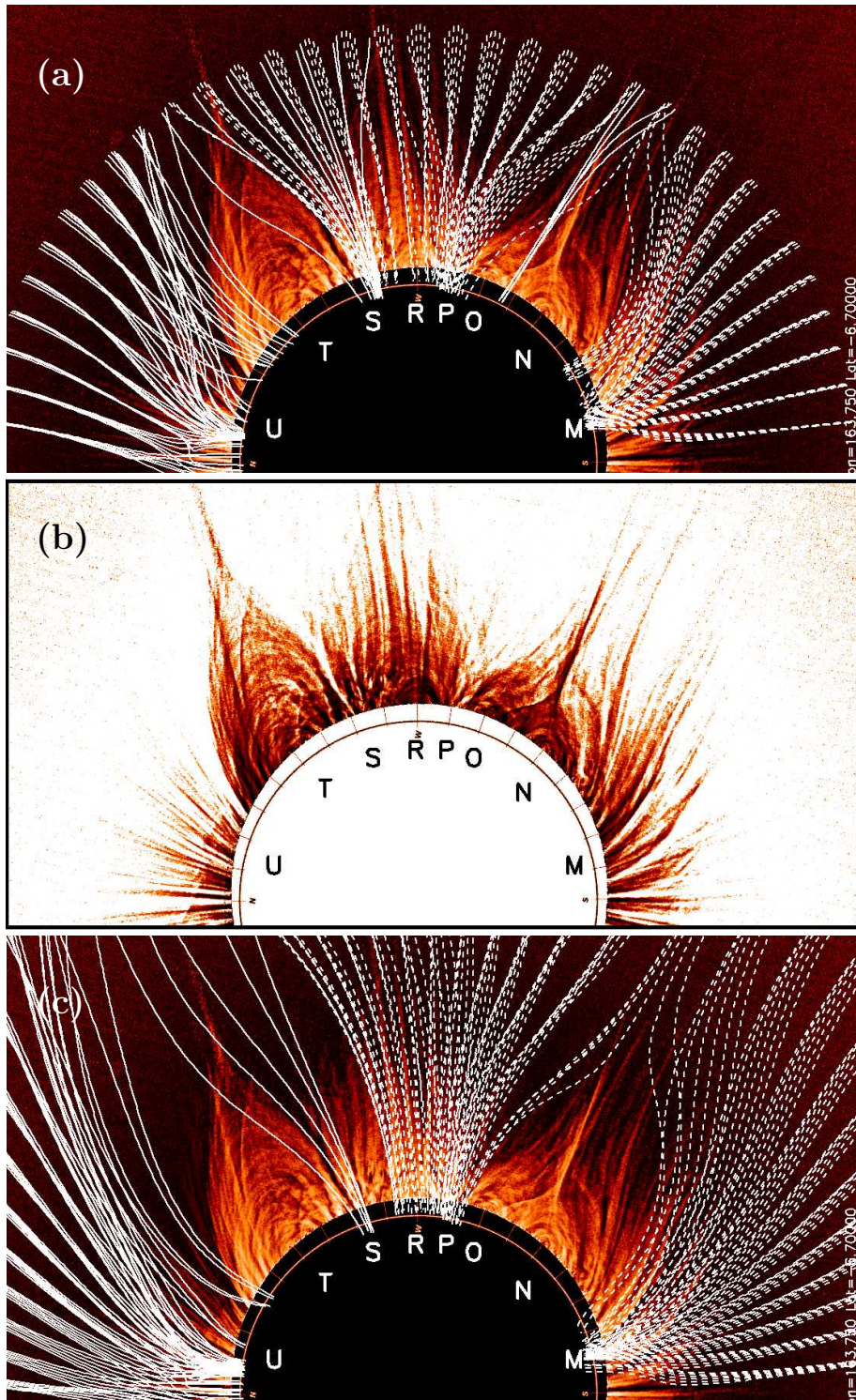
Figure 8. Open field lines similar to those in Figure 7, prepared for the west limb. The north pole is on the left and pictures show position angles in the range from 180° to 360°.
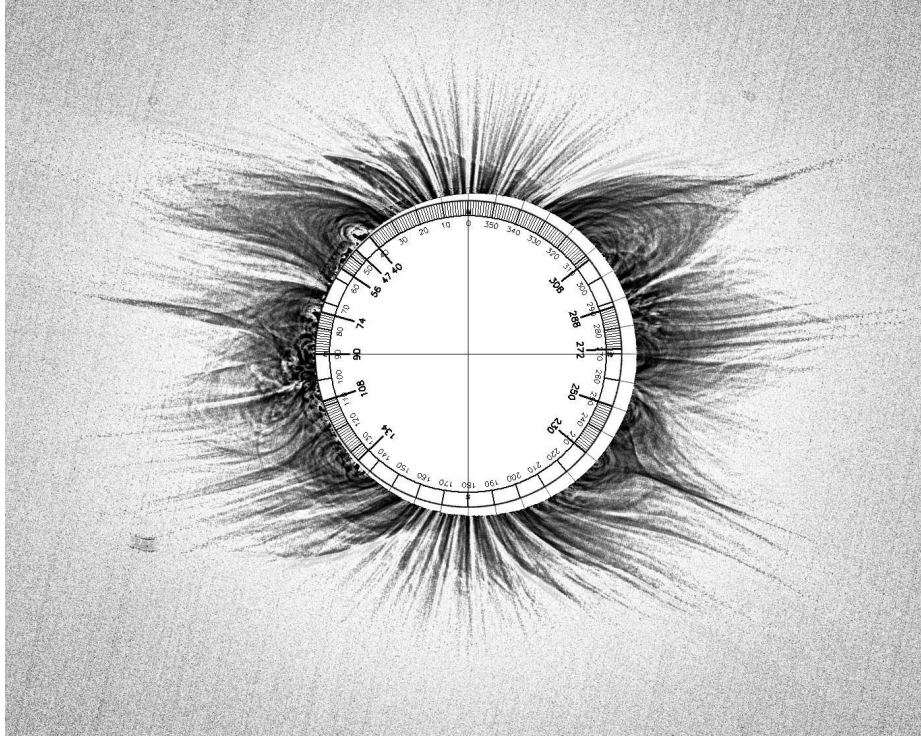
Figure 9. Processed white-light fine coronal structures presented as negative copy. The large-scale magnetic polarity distribution on the limb-line is demonstrated in the annulus depicted inside the limb circle. The positive polarity is radially hatched; neutral-line positions are shown by bold lines labeled by position angle measured from the north pole counterclockwise.

limb line. In the observation plane related to the limb they are located between labels "G" and "H".

3.1.2. Open Structures on the West Limb

The west-limb open structures are modeled in Figure 8 under similar conditions as in the East. Open field lines are rooted in four separate regions, characterized as the coronal holes.

Around the south pole above the label "M", the open field lines related to negative polarity are generated from the south polar coronal hole not extending below latitude $-60°$. On the processed picture of the corona one can find about 18 discrete fine structures. Many of them are not clearly divided or distinguished. The visibility is limited to a distance from $0.9R_\odot$ to $1.3R_\odot$.

A similar system of open field lines related to positive polarity is also around the north pole and is labelled "U". Along the limb line the open structures, region exceeds latitude $55°$. The observed open rays are distinguished by the distance $0.9R_\odot$ and about 15 discrete rays are observed.

A specific funnel-shaped system of the field lines can be found in the equatorial region where above the labels "P" and "R" the very extensive coronal hole with

a latitude range from N15° to S30° cross the limb line and relate to negative polarity.

The positive open field region above the label "S" is about 26° in longitude in front of the limb line.

3.2. Closed Structures

We observe closed structures above the intersection points of all inversion lines of the large-scale magnetic fields with the limb-line. A general view of all systems above the limb is presented in Figure 9. The closed structures are represented by arches rooted in the photosphere in neighboring large-scale regions with opposite polarities. The sufficiently high resolution of the processed image avoids analyzing the both internal and external parts of the structures. Individual systems of the closed structures are presented in detail in Figure 12. The corresponding selection of the field lines, computed according to the HCSS model for two values of the source surface radius is presented in Figures 10 and 11.

3.2.1. Closed Structures above the East Limb

The coronal structures observed above the east limb are presented in Figure 10. The magnetic field lines were calculated only from selected starting points in the photosphere displaced in a relatively narrow sector ±20° in longitude on both sides of the the limb-line position.

The bright streamer between position angle values 27°−63° looks like a typical helmet streamer with prominence and a dark dome (cavity) inside. The whole streamer, however, has a complicated structure. Detail of the processed picture is shown in Figure 12a. The high prominence within the position angle interval 39°−47° is a projection of a long polar crown filament, clearly discernible also on the disc in line Hα. An easily observable loop structure and dark cavity around the prominence is also found on the unprocessed images and is labeled in Figure 10 by "C". The good contrast of the whole phenomenon is probably caused by the fact that the inversion line between the positive polar magnetic region and the narrow strip island of negative polarity on latitude N48° is oriented strictly along the line of sight (perpendicular to the limb line; see Figure 6). Topology of the magnetic flux distribution in the photosphere below the streamer is complex. As seen in Figure 6 the footpoints of all open structures are rooted in positive polarity and also on the disc in Figure 7 where nearly all open structures, covering a substantial part of the streamer, also indicate positive polarity.

The low contrast part of Figure 12a above the polarity inversion line at position angle 56° shows small prominences and arches (in Figure 10 labeled as "D""). Arches interconnect the small island of positive polarity which is present mainly on the disc with a negative polarity at position angles 45° – 47°. Orientation of the inversion line is inclined to the limb from the line of sight for about 15°, and we observe this system (prominence as well as the corona) in a projection from the northern side.

The orientation of whole streamer is far from radial. The inclination of their axis from a radial direction is about 33° to the solar equator. Also the length
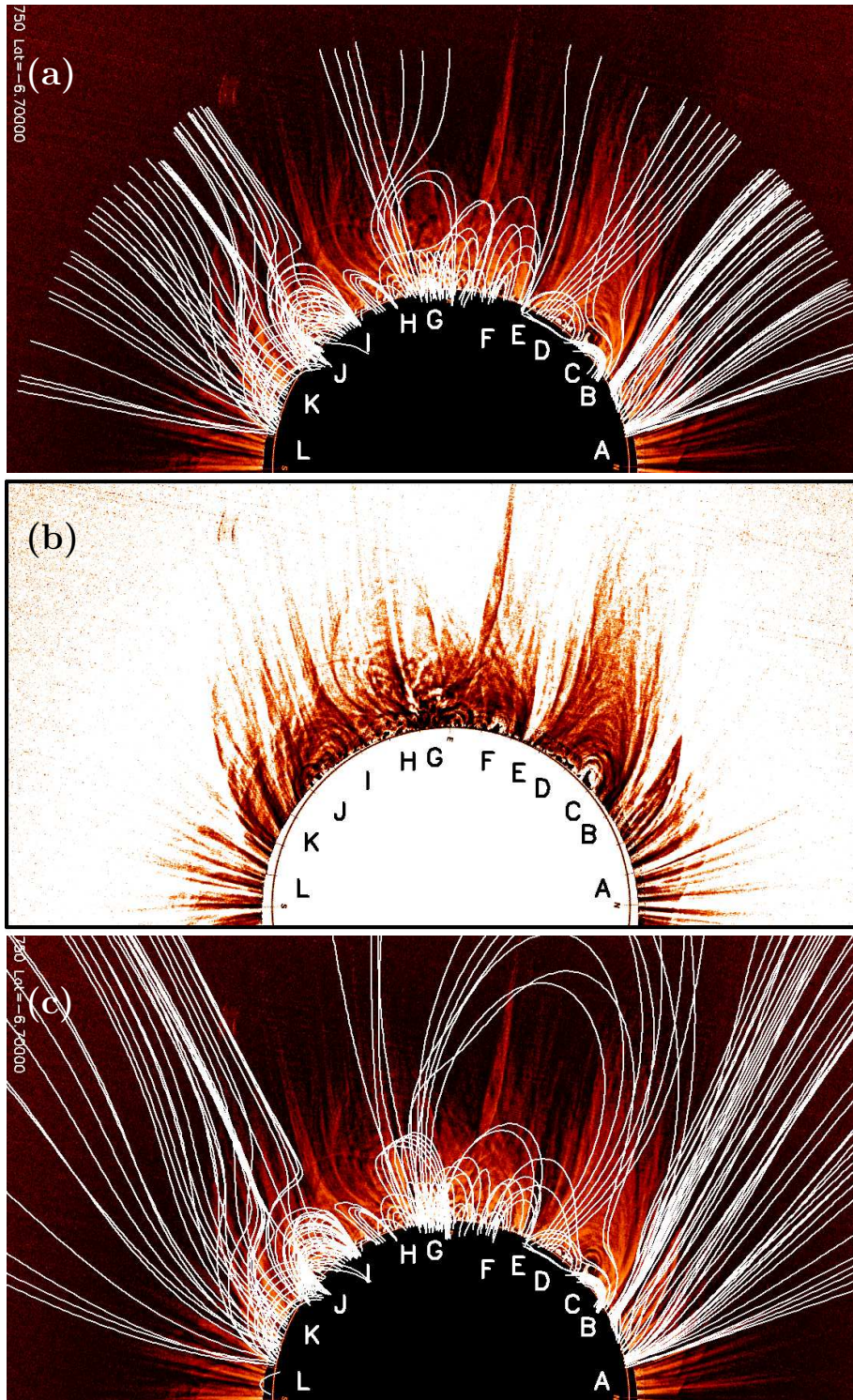
Figure 10. Selected field lines for the east limb plotted over the coronal structures, computed according to the HCSS model for source surface radius (a) $R_{ss} = 2.5R_{\odot}$ and (c)$R_{ss} = 4.0R_{\odot}$. In contrast with Figures 7 and 8, the field lines were selected according to an optimal fit with fine structures observed close to the solar limb. Image (b) in the center shows processed coronal structures. The north pole is on the right and photos show position angles in the range from $0°$ to $180°$.
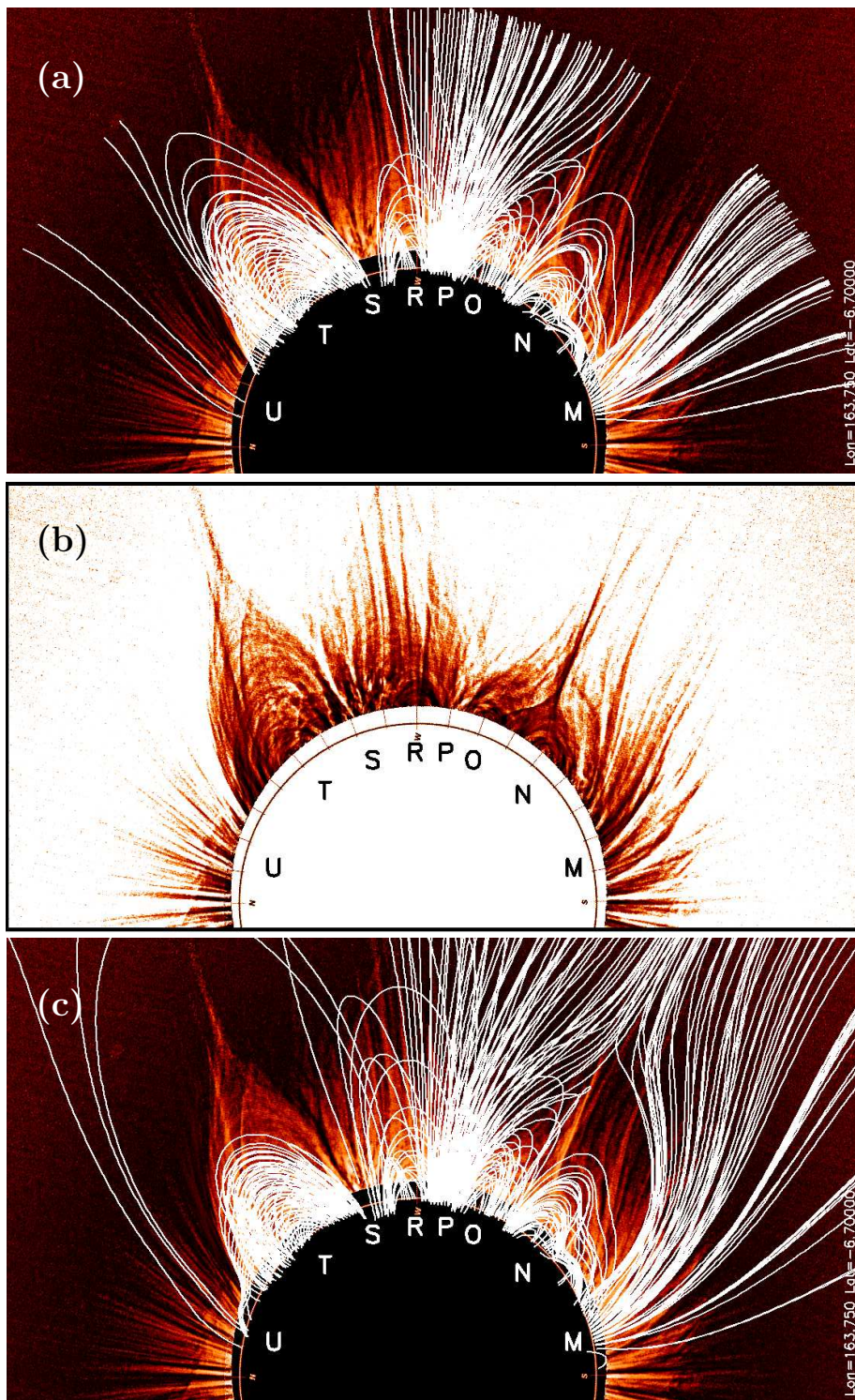
Figure 11. Selected field lines above the west limb. The image is organized similarly to Figure 10. The north pole is on the left and pictures show position angles from 180° to 360°.
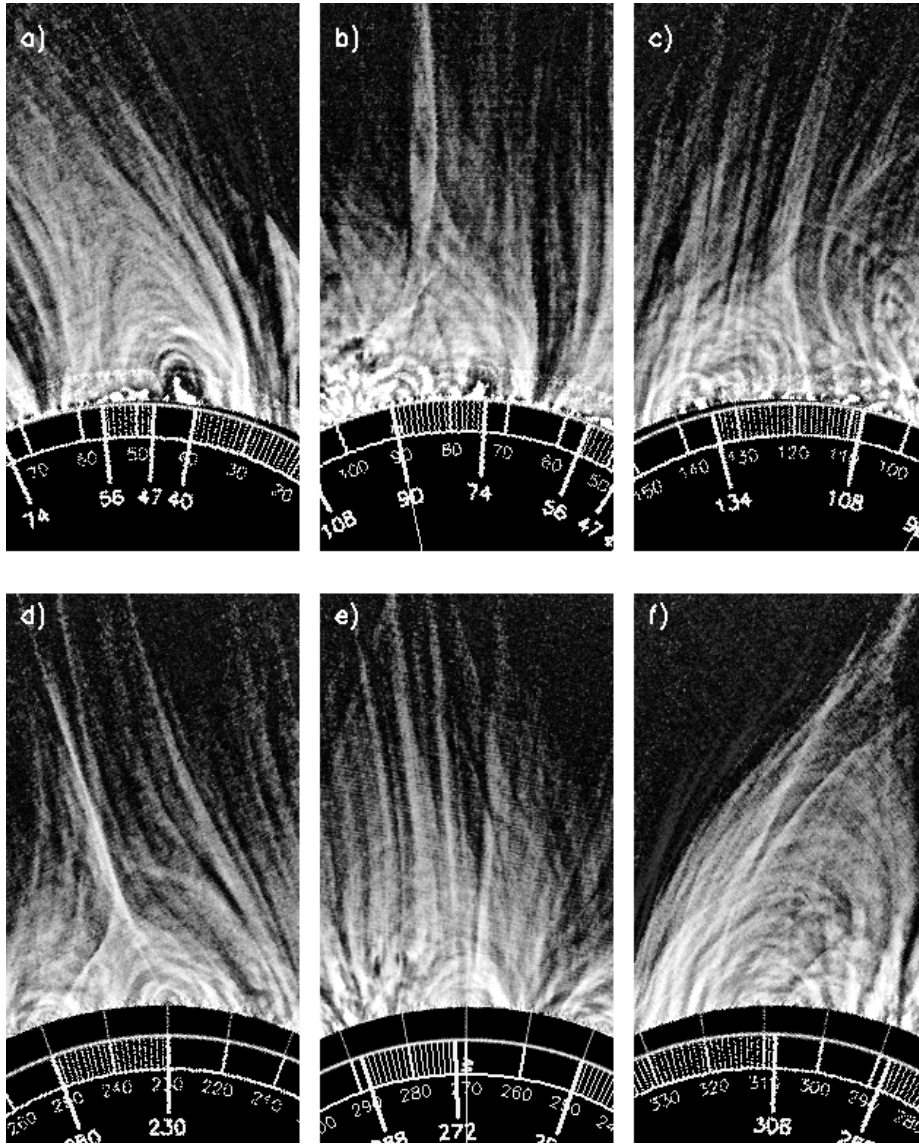
Figure 12. Closed structures selected above the limb during the total solar eclipse on 29 March 2006. Photos are centered on position angles 50° (a), 78° (b), 120° (c), 230° (d), 270° (e), and 310° (f) and show the fine structures up to $1.2R_\odot$ above the solar limb. Individual structures are described in the text.

of this streamer is extreme and a not very typical cusp is detected on the radius $4.5R_\odot$ from the solar center. Open structures, ranging the streamer from both sides are influenced by a magnetic field described by low-order spherical harmonics, which dominate in creating a global structure of the corona. Due to the presence of only the positive polarity in open structures, the term "pseudostreamer", introduced by Wang *et al.* (2007), can be accepted.
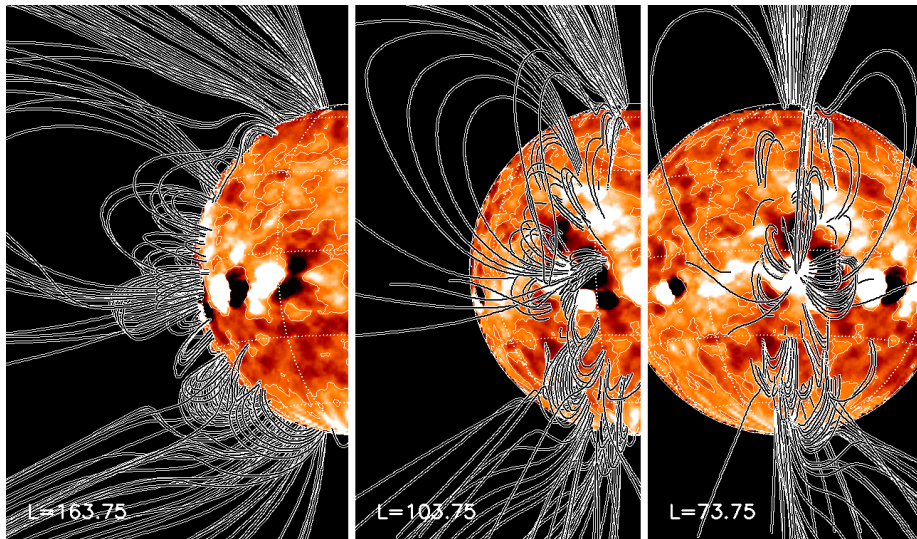
Figure 13. A selected set of the field lines corresponding to coronal structures observed on the east limb on the left. L is the heliographic longitude of the disc center. Rotated views for 30° and 90° are depicted from left to right.

A specific object observed is the giant bubble-like structure above the label "G" in Figure 10 which was also observed by Pasachoff *et al.* (2007) and by Habbal *et al.* (2007) in Fe XI 789.2 nm. From the HCSS model we are not able to compute the corresponding field line structures. Only the loop system above labels "G" and "H" in Figure 10c which is related to opposite polarities near an active region is located in the center of the projected bubble.

At the position labeled in Figure 10 near the limb as "F" we also observe another prominence and between position "F", "G", and "H" a loop system near the limb coincides with field-line loops generated from the model. Position "G" is very complex and position "H" connects the limb by open lines with the source surface. As can be seen in Figure 6, the complex coronal structure above label "G" relates to the presence of the active region with a strong magnetic field.

The second system with closed structures is related to inversion lines at position angle 74° and 90° in Figure 9 and presented in detail in Figure 12b. Above the inversion line at position angle 74° (N16°) we observe a prominence surrounded by a small cavity and by an arch system. The inversion line on the disc is inclined from line of sight from about 28° southward. The second inversion line at position angle 90° is inclined from the line of sight by about 8° northward. Separate arch systems are complex, because we observe both from different aspect angles. The summit of both arch systems is about $0.2R_\odot$ above the limb. Upwards the fine structures have a tendency to create cusps, but individually for each arch. The most prominent phenomenon is a bright streamer observed above position angle 82° and detectable on our processed image out to $4.5R_\odot$ from solar center and on SOHO/LASCO-C2 Coronagraph out to distance $6.2R_\odot$. This stream evokes the impression that the internal structure is helically
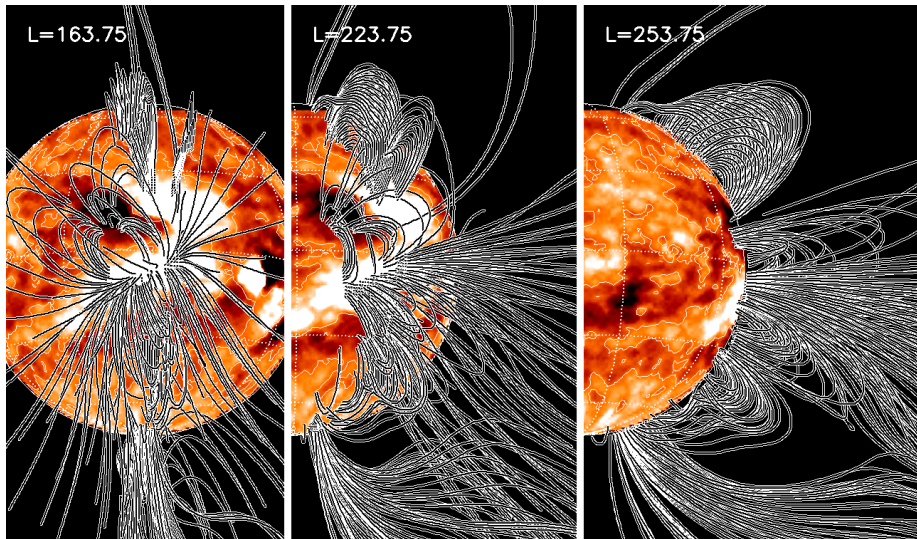
Figure 14. Rotated view of the selected field lines on the west limb. L is the heliographic longitude of the disc center. Limb position during the total eclipse is on the right and the two other pictures with an equal set of field lines are rotated by 30° and -90° from right to left.

twisted along a radial direction. From our HCSS model, however, we are not able to compute such a structure.

The inner corona above the limb in the position angle interval $65° - 145°$ is very dramatically structured by a magnetic field in the photosphere, where a complex field structure is present with a strong field of both polarities as well as with well developed background magnetic regions NOAA 10866 and 10867.

The last dominant closed structure is, as shown in Figure 9, on the southeast limb related to magnetic inversion lines on position angles 108° and 134°. The inclination of the inversion line from the line of sight near the limb is 45° and 22°, respectively. A detailed structure of the corresponding limb sector with corona is found in Figure 12c. Two arch systems, both corresponding to inversion lines are present. Their structure is very fine and mainly the system relating with a highly inclined inversion line at 108° can probably be observed from the side. The relating magnetic-field lines computed for this situation are shown in Figure 10 labeled "I" and "J". The second arch system is above label "K". Both systems are superposed by many open structures related only to negative polarity. In Figure 10c (for, $R_{ss} = 4.0R_{\odot}$), the specific structure of open field lines above labels "I" and "J" is given by the fact that footpoints of lines above "I" are behind the limb line (about 25° – 40°) and relate to a coronal hole in latitude range S(0° – 25°), whereas above "J" and mainly above "K" all field lines are rooted in the southern coronal hole.

3.2.2. Closed Structures above the West Limb

Fine coronal structures on the west limb are rather simpler than on the East. The main reason is that distribution of the magnetic flux in the photosphere

near Carrington longitude 253° is without new strong fields and the extended old large-scale background bipolar magnetic regions dominate.

The polar plumes and narrow rays are labeled by "M" on the southern and "U" on the northern hemispheres.

On the southwest limb two different arch systems are present. These are related to two intersections of the inversion lines with limb-line as shown in Figure 9 at position angles 230° and 250°. Inclinations of the inversion lines to the line of sight are for both 10° and 8° respectively. Details are presented in Figure 12d. In Figure 11 above label "O" shows they have their summit only $0.18R_\odot$ above the west limb. Another system above the label "N" is dominant and complex. The clearly observed arch system has its summit $0.23R_\odot$ above the west limb. However, above the summit of arch systems the cusps and streamers up to a distance of $2.5R_\odot$ from solar center are detectable. This is inclined relative to radial direction for 15°.

Above the Equator (in Figure 11 label "R") is a well-observed arch system with two different characteristic structures. Both relate to points of the inversion line on the limb according to Figure 9 on position angles 272° and 288°. Details are provided in Figure 12e. The first one is typical of low-lying compact arches with a projected summit about $0.26R_\odot$ above the west limb. The inversion line is inclined only 8° to line of sight. The arch system above this limit seems to be transformed into a cusp and open system, probably containing the current sheet.

The second system is less compact and the highest identified arch has its summit $0.63R_\odot$ above the limb. The inversion line has a great inclination to the line of sight, about 46°.

A dominant coronal phenomenon above the northwest limb is shown in Figure 11 above the label "T". It is a typical helmet structure with many arches below the cusp point. A phenomenon relates to the presence of the inversion line at position angle 306° as can be seen in Figure 9. Details of the helmet structure are shown in Figure 12f. Observations above the limb are a superposition of many similar arches distributed along the line of sight. The mean inclination of the inversion line from line of sight is 31°. The footpoints of all arches are rooted in two large-scale magnetic regions of the opposite polarity located between the north pole and the middle north latitudes.

3.2.3. Selected White-Light Structures and the EUV Images of the Corona

We use the field lines selected according to the optimal fit with the white-light corona structures on the east limb in Figure 10 as testing structures with the corona observed in EUV on wavelength 17.1 nm (Fe IX/X) from SOHO/EIT (Delaboudinière *et al.*, 1995). The picture from 4 April 2006 with disc center position 87.3° and 6.4° in heliographic longitude and latitude, respectively, is shown in Figure 15. Field lines, indicating the bright fine structures in the white-light corona on the limb are transformed by rotation to the corresponding position on the disc, which can be compared with the EUV coronal structures. The high-temperature EUV fine structures usually close relate to photosphere loop systems, enhanced mainly in the active regions with concentrated magnetic field.
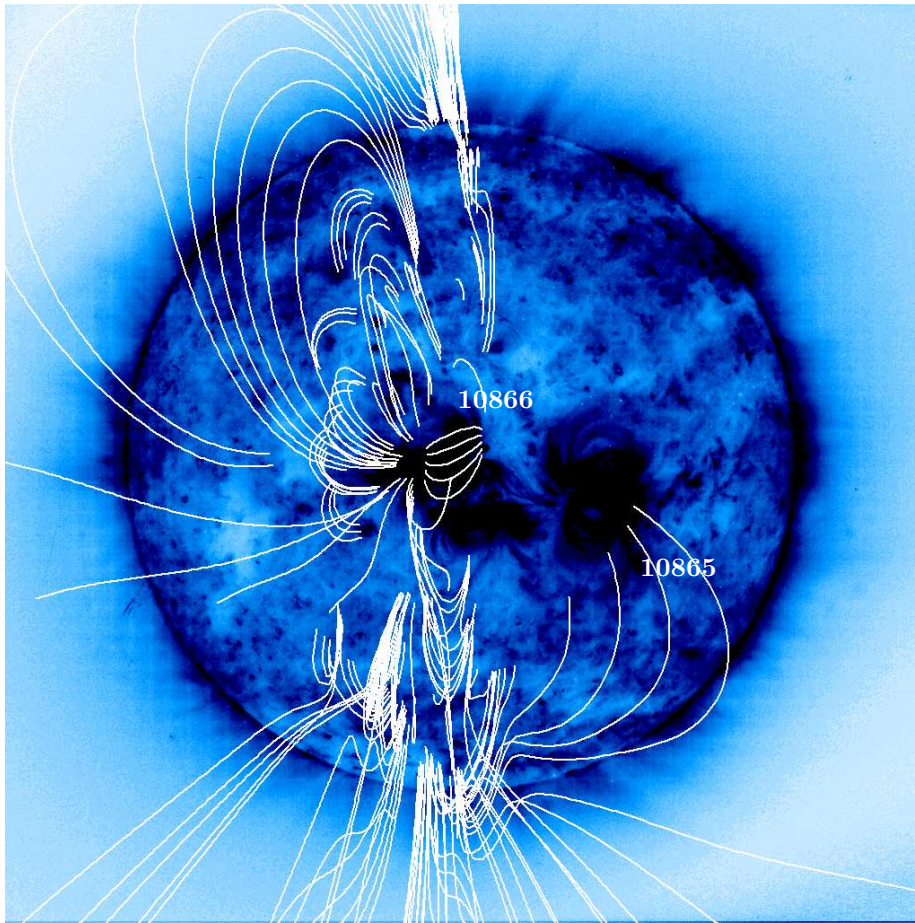
Figure 15. The selected field lines transformed from the east limb into position on the disc about seven days later. Lines are superposed on the SOHO EIT 17.1 nm (Fe IX/X) picture from 4. April 2006 at 07:00:16 UT.

The EUV loops and arches are usually low, not exceeding a height of $0.22R_\odot$. On the other hand, our selected field lines are usually higher than $0.25R_\odot$. Above active regions NOAA 10866 and 10867 near the east limb, the arch-like structure of the field lines and then also of the white corona arches continuously follows the shape of corresponding structures in the EUV. The other field lines are present in regions with a weak magnetic field and in the EUV they do not have corresponding arch structures. However, in nearly all cases, the footpoints of the field line arch systems correspond well with a brightness enhancement in the EUV. Enhancement corresponds with a peak temperature of 1.3 MK in the footpoints of the identified coronal structures.

A similar reconstruction for the west-limb field lines is shown in Figure 16. The disc center for 23 March 2006 is nearly free of the active region strong fields
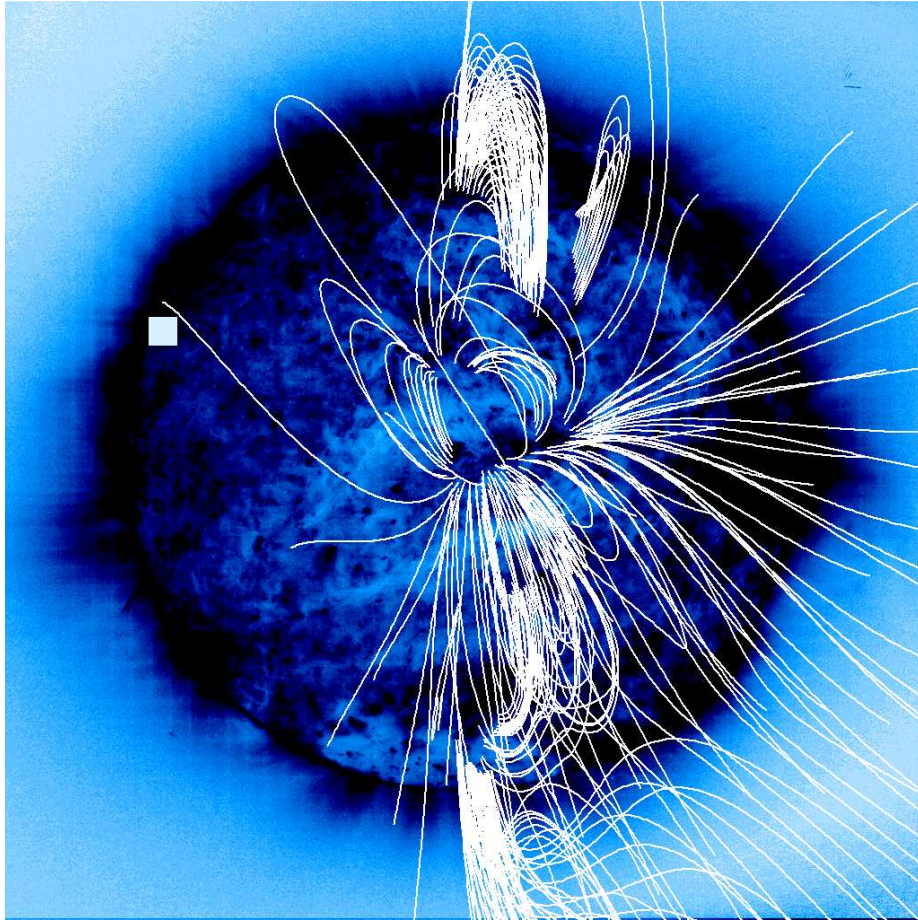
Figure 16. The selected field lines transformed from the west limb into position on the disc about 6 days earlier from 23 March 2006 in 07:00:15 UT. Lines are superposed on the SOHO/EIT 17.1 nm (Fe IX/X) picture of the Sun.

and only well developed large-scale bipolar magnetic regions are present. The arch structures connected with helmet are for selected field lines modeled near the north limb. Similarly, as on the east limb, all field lines relate to white light coronal structures rooted in bright enhanced regions in a hot low solar corona. The same local differences are caused by lower resolution of the used magnetic fields than SOHO/EIT images. The selected open structures cover an extended part of the south hemisphere.

4. Discussion and Conclusions

The coronal structures observed during the total eclipse are projected onto the observing plane from about a 50° broad sector in longitude on both east and west limbs. An image of the corona after processing provides enhanced fine rays,

arches, loops, and streamers with spatial resolution usually lower than 10 arcsec (details > 8Mm) due to telescope parameters and atmospheric conditions. We can not rule out that all of the objects described are composed of finer threads than those discovered by November and Koutchmy (1996) and which remain still unresolved for us.

The topology of the large-scale magnetic field in the photosphere is crucial for the structure of the coronal field formation. Global magnetic-field distribution in the outer corona is characterized by the position of the heliospheric current sheet at the distance from $3R_\odot$ to $5R_\odot$, where usually the source surface with an outer boundary condition is located. The fields we extrapolate from magnetic flux distribution in the photosphere and according to the low order spherical harmonics of the solar magnetic field in photospheric regions with dominant positive and negative polarities are present. Distribution of the global structures evolves only slowly in time.

Closed structures are connected with two opposite polarity regions. Below the heliospheric current sheet we usually observe only the typical arches with helmet streamers above the cusp point detected recently also by Woo and Habbal (2005). In this structure the mechanism described by Pneuman and Kopp (1971) is confirmed. More complex large-scale topology originates when in a large-scale unipolar region a new flux emerges and forms an island of opposite polarity. Such an island evolves in time and changes its shape and magnetic field intensity. Above inversion lines we observe the arch systems which near the limb are superposed together and create a complex image of coronal fine structures due to their heterogeneous orientation. The island of one polarity surrounded by a more extended and dominant opposite polarity is usually responsible on the limb minimally for two arch systems apart, with a pair of legs in a common polarity island and two extended legs in the surrounded dominant opposite polarity. This kind of configuration previously studied by Koutchmy *et al.* (1994) is not rare on the limb and the HCSS model indicates such configuration above both limbs on the south hemisphere.

For many individual closed structures above a summit of their loops and arches the cusp structures are observed. Many of them suggest the jets observed for some structures in flares (Shibata *et al.*, 2006). Their basic orientation is quasi-radial and they seem to have helical structures (or to be twisted) along the vertical axis. We are not able to derive the cusp and helical jets in our HCSS magnetic model. Configuration with streamers rooted on sides in equal polarity Wang, Sheeley, and Rich (2007) describes as pseudostreamers.

We consider the alignment of the modeled field lines with the processed white light coronal arches to be very good. Many of the field lines computed and plotted above the limb have a shape that coincides with the position and orientation of the open as well as closed fine coronal structures. At the same time the coronal structures overlap and consist of different systems projected along the line of sight. Spatial resolution of the processed images of the white-light corona is limited and we found about 200 of the well-coinciding field lines. In the present paper the term "well coinciding" means that the computed field-line projection into the observing plane overlaps the observed fine structure in the processed picture of the corona. The coronal structure itself is usually wider than

a computed field line and frequently it is not entirely continuous. It is usually more distinct and brighter close to the solar limb than above $1.4R_{\odot}$ from solar center. The combination of the field lines with the EUV corona photographs show spatial consistency of the white-light and EUV coronal arches as well as a close relationship of white-light coronal structures in their foot points with enhanced brightness in EUV corona. The 3D spatial model of the middle corona based on the white-light observations is more complete.

Open structures in the processed images of the eclipse corona relate predominantly to the coronal plumes emanating from the coronal holes around both poles as well as from small holes in the activity zone. Structures in the observed plane are projected together along lines of sight. Plumes in polar regions in their bottom part are usually overlapped by structures related to large-scale magnetic field in middle latitudes. Above the limb we observe the fine structures rooted in coronal holes located in heliographic coordinates around $\pm 20°$ far from the limb line.

The open magnetic field lines with only a radial field cover the whole sphere with $4R_{\odot}$ to $5R_{\odot}$. In the photosphere the open field lines are rooted in separate small areas in large-scale unipolar magnetic regions. The rest of the surface area creates a base for many closed structures. Usually the space with closed structures is much denser than space with open structures and creates large-scale regions with enhanced brightness.

Problems with complete alignment of observed and computed structures in the intermediate space between the closed and nearly linearly open structures from the center of coronal holes reflect that the HCSS model, as the numerical method of the magnetic field extrapolation, has a limited capability. The model is fully static and does not include any velocity fields of horizontal transport of magnetic flux in the photosphere as well as the vertical transport due to the solar wind. Our model is not able to calculate the helmet or cusp structures influenced by coronal expansion. The method is "quasipotential" and in fact is current-free except for the parameterized horizontal current, constant for the whole Sun and perpendicular to gravity. A similar method for basic computations is usually used also in a more sophisticated MHD approach (Mikic *et al.*, 1999) as the initial configurations for development of the final configurations. Good agreement between observed white-light coronal structures and the static and nearly current-free modeled configurations lead to the conclusion that all closed structures in the corona except those in active regions with young and dynamically evolving magnetic fields have only a negligible departure from current-free configurations.

There are two observed coronal phenomena which we are not able to construct according to our model.

The first relates to a large prominence and to the system of arches above them. We are not able to generate the shape of field lines correctly from our magnetic model even when we try to adjust free parameters R_{ss} and a over the broad range. The observed arches are distinctly higher than the computed ones. We suppose that in this region the simple global HCSS model is not satisfactory and that only a local increase of horizontal current characterized by the parameter a can help. Another option for explaining the disagreement can also be the low

quality of the magnetic data in this part on the east limb, because for a few days while covering the area of the east limb no data from observations were available and the magnetic data for spherical-harmonic-coefficient evaluation were partically extrapolated.

We are not able to create the observed shape of bubble above the east limb between the Equator and latitude S24° by the HCSS steady state model, and therefore we suppose that the object is probably temporarily unstable and modeling them needs another approach. In any case we cannot rule out that the initial stage of the bubble-like structure was related to the activation of the closed structure partly rooted in an active region. The observed bubble-like structure is not typical for closed coronal stable structures connecting two opposite polarities in the photosphere. This phenomenon was observed from Libya and Turkey in the course of about 69 minutes. Later observations from Asia were processed by another procedure, their spatial resolution is lower and they do not contain similar information.

A close relationship between computed magnetic-field lines and the observed open and closed coronal structures shows that coronal phenomena very probably co-rotate within the photosphere underlying magnetic fields. Interpretation of statistically obtained differences between rotation rates of magnetic patterns in the photosphere and the rotation rates of corona need improvement. With a real difference of rotation rates, a systematic deformation of coronal fine structures is inevitable, whereas with co-rotation a good fit of the current free model with observed coronal details is confirmed.

References

Altschuler, M.D., Newkirk, G.: 1969, *Solar Phys.* **9**, 131.

Bogdan, T.J., Low, B.C.: 1986, *Astrophys. J.* **306**, 271.

Delaboudinière,J.-P., Artzner,G.E., Brunaud,J., Gabriel,A.H., Hochedez, J.F., Millier, F., Song, X.Y., Au, B., Dere, K.P., Howard, R.A., Kreplin, R., Michels, D.J., Moses, J.D., Defise, J.M., Jamar,C., Rochus,P., Chauvineau,J.P., Marioge,J.P., Catura, R.C., Lemen, J.R., Shing, L., Stern, R.A., Gurman, J.B., Neupert, W.M., Maucherat, A., Clette, F., Cugnon, P., Van Dessel, E.L.: 1995, *Solar Phys.* **162**, 291.

Druckmüller, M., Rušín, V. and Minarovjech, M.: 2006, *Contrib. Astron. Obs. Skalnaté Pleso* **36**, 131.

Galal. A.A., Soliman M.A., Hamid R.H., Semeida M.A., Sabry M., Elminir H.K., Abdel Moneim K.M., Marzoke B.A.: 2006, *NRIAG Journal of Astronomy and Astrophysics (Special Issue)*, 103.

Habbal, S.R., Morgan, H., Johnson, J., Arndt, M.B., Daw, A., Jaeggli, S., Kuhn, J., Mickey, D.: 2007, *Astrophys. J.* **663**, 598.

Koutchmy, S., Koutvitsky, V.A., Molodensky, M.M., Soloviev, L.S., Koutchmy, O.: 1994, *Space Sci. Rev.* **70**, 283.

Loucif, M.L., Koutchmy, S.: 1989, *Astron. Astrophys. Suppl.* **77**, 45.

Mikic, Z., Linker, J.A., Schnack, D.D., Lionello, R., Tarditi, A.: 1999, *Phys. Plasmas* **6**, 2217.

Nakagawa, Y., Raadu, M.A.: 1972, *Solar Phys.* **25**, 127.

November, L.J., Koutchmy S.: 1996, *Astrophys. J.* **466**, 512.

Pasachoff, J.M., Rušín, V., Druckmüller, M., Saniga, M.: 2007, *Astrophys. J.* **665**, 824.

Pasachoff, J.M., Rušín, V., Druckmüller, M., Druckmüllerová, H., Bělik, M., Saniga, M., Mi-
    narovjech, M., Marková, E., Babcock, B.A., Souza, S.P., Levitt, J.S.: 2008, *Astrophys. J.*
    682, 638.

Pneuman, G.W., Kopp. R.A.: 1971, *Solar Phys.* **18**, 258.

Shibata, K., Ishido, Y., Acton, L.W., Strong, K.T., Hirayama, T., Uchida, Y., McAllister, A.H.,
    Matsumoto, R., Tsuneta, S., Shimizu, T., Hara, H., Sakurai, T., Ichimoto, K., Nishino, Y.,
    Ogawara, Y.: 1992, *Pub. Astron. Soc. Japan* **44**, L173.

Schatten, K.H.: 1971, *Cosmic Electrodynamics* **2**, 232.

Schulz, M., Frazier, E.N., Bouchner, D.J.: 1978, *Solar Phys.* **60**, 83.

Wang, Y.-M., Muglach, K.: 2008, *Solar Phys.* **249**, 17.

Wang, Y.-M., Sheeley, N.R.Jr. : 1992, *Astrophys. J.* **392**, 310.

Wang, Y.-M., Sheeley, N.R. Jr. and Rich, N.B.: 2007, *Astrophys. J.* **658**, 1340.

Wang,Y.-M., Biersteker, J.B., Sheeley, N.R. Jr., Koutchmy, S., Mouette, J., Druckmüller, M.:
    2007, *Astrophys. J.* **660**, 882.

Wiegelmann, T.: 2004, *Solar Phys.* **219**, 87.

Woo, R.: 2006, *Astrophys. J.* **639**, L95.

Woo, R., Druckmullerová, H.: 2008, *Astrophys. J.* **678**, L149.

Woo, R., Habbal, S.R.: 2005, *Astrophys. J.* **629**, L129.

Zhao, X., Hoeksema, J.T.: 1993, *Solar Phys.* **143**, 41.

Zhao, X., Hoeksema, J.T.: 1994, *Solar Phys.* **151**, 91.